Estimating the dose differences nearby the metal implant
by means of artificial contouring errors via Monaco and Geant4

G. Bakıcıerler^{a,b,*}, G. Şişman^a, and K. Akgüngör^c

^{a}*Dokuz Eylul University, Institute of Health Science, Department of Medical Physics,*
35530, Narlidere, Izmir, Turkey.
**e-mail: gizem.bakicierleraybars@ogr.deu.edu.tr; gizem.sisman@ogr.deu.edu.tr; kadir.akgungor@deu.edu.tr*
^{b}*Celal Bayar University, Faculty of Medicine, Department of Radiation Oncology,*
45030, Yunusemre, Manisa, Turkey.
^{c}*Dokuz Eylul University, Faculty of Science,*
Department of Physics, 35390, Buca, Izmir, Turkey.

Metal artifacts cause errors in the exact delineation of implants and dose changes in radiotherapy. In this study, the dose distribution differences in the region of interest (ROI) were calculated by deliberately making contouring errors from the real size of model implants by using both Monaco treatment planning system (TPS) and Geant4 toolkit. In Sec. 2, the computed tomography images were acquired by placing known uniform cylindrical geometry titanium (Ti6Al4V) and cobalt (CoCrMo) alloys into water phantoms separately. The metal alloys were artificially contoured as 2 mm contracted and expanded from their real dimensions in Monaco TPS. The plans were generated with 6 MV photon beams for contouring of three different sizes, real, contracted and expanded, for each metal alloy. In addition, all configurations were simulated in Geant4 by using the photon energy spectrum data of the Elekta Synergy linear accelerator. Then, the 3D dose data obtained from ROIs near the implant in Monaco TPS and Geant4 were analyzed with in-house programs. In Sec. 3, the depth dose values of Geant4 were compatible with TPS calculations and ion chamber measurements. When the alloys were contoured to real dimensions, it was observed that the local isodose values have changed up to 15% in ROI. The mean dose values were found to be higher in contracted and lower in expanded contours. It was observed that ± 2 mm error in contouring the implants changed the mean dose up to $\pm 8\%$. In Sec. 4, this study emphasized that a few millimeters of error in contouring different implant materials can have a significant effect on dose distribution in a region close to the implant.

Keywords: Monte Carlo simulation; Monaco TPS; implant; contouring.

1. Introduction

The number of patients, who have metallic implants such as mandibular plates, dental fillings, spinal cord fixation devices, surgical rods, stents, upper and lower extremity prostheses that require radiotherapy due to various malignancies, have been increasing in recent years. All the materials used in the implants have high atomic numbers and density; therefore, they tend to significantly affect target and normal tissue doses in the treatment region to be irradiated [1].

The variation of the dose changes, which is caused by the implants with high atomic number regarding factors like energy, material, geometry and thickness, have been revealed by the researchers via experimental and calculation methods [2–7]. In the literature, absorbed dose distributions have been evaluated by methods such as film dosimetry, different clinically used treatment planning system (TPS) algorithms, and Monte Carlo (MC) simulations. It has been observed that when the incident photon interacts with a high electron density material placed in water or tissue-equivalent medium, dose increase due to upstream backscattering and dose perturbation below the implant occur [8–12].

The implants with high atomic number reveal significant artifacts in reconstructed computed tomography (CT) images. Kovacs *et al.* studied metal artifact reduction techniques in order to determine the effects of radiotherapy on tumor description on CT images of phantoms containing various metal implants [13]. Byrnes *et al.* used different metal implant materials with known geometries to eliminate geometric uncertainties. They determined the errors in the dose calculation were caused by the Monaco MC algorithm from different electron density without the effects of incorrect contouring [14]. The dose distributions resulting from the effect of artifact and high electron density have been measured and calculated by researchers using MC methods [1, 15]. As a result, these implants cause difficulties to determine the contours of the object and calculating the correct dose distribution within the patient.

Delivering the prescribed dose to the patient with an accuracy of $3-4\%$ is the key component of the achievement for the radiation therapy [16, 17]. Modern advances in radiotherapy have increased the accuracy of dose delivery [18]. The most important constituent of TPSs is accurate dose calculation [19]. Therefore, the use of MC calculation algorithm in commercial TPS has become widespread recently [14] since

it is the most accurate approach in determining the dose released by ionizing radiation in a medium. This technique offers powerful numerical solutions to the highly complex problems. In radiotherapy, it has been proven mathematically that they are more advantageous than analytic algorithms in solving problems with many parameters, such as calculating the patient dose, specifically in regions with high density materials [20–23]. The usage of MC calculation algorithm provides the ability to calculate more reliable dose levels, especially in heterogeneous environments with high density implants to TPS [1, 24–28]. In addition to this, MC simulations allow to obtain accurate and detailed information in order to evaluate dose distributions in TPS [2].

Although TPS applies different correction factors to artifacts, it is very likely to make errors and misjudgments to determine the boundaries of implants by the observer. It is important to determine on what scale these errors would affect the dose calculations. Thus, planners and physicists are able to understand the uncertainties that exist and gain in dose delivery to target volumes and better sparing of organs at risk [14]. However, there has been no report on how metal implants should be contoured nor a study that would reveal the effects of certain errors in contouring on dose distribution. The aim of this study is to evaluate the dose change caused by deliberate contouring errors in the exact delineation of implants in the region of interest (ROI) near the implant by using both Monaco TPS and MC simulation with the Geant4 [29] toolkit.

2. Materials and methods

2.1. The physical and chemical properties of the materials

In order to eliminate the errors related to determination of density and boundaries due to the artifacts that high atomic number heterogeneity may reveal in CT images, implant materials with uniform geometry of known densities and dimensions were used. The implant materials were obtained from commercially available samples of titanium (Ti6Al4V) and cobalt (CoCrMo) alloys. The metal alloys with uniform cylindrical geometry were selected as 150 mm in height and 32 mm in diameter for Ti6Al4V and 29 mm for CoCrMo. Ti6Al4V alloy contains approximately 89.95% titanium, 5.80% aluminum, 3.92% vanadium and also trace amounts of hydrogen, carbon, nitrogen, oxygen, iron. CoCrMo alloy contains 65.35% cobalt, 27.2% chromium, 5.39% molybdenum and trace amounts of carbon, nitrogen, silicon, nickel, iron as well. The physical densities of Ti6Al4V and CoCrMo alloys are 4.43 g/cm^3 and 8.30 g/cm^3, respectively.

2.2. CT simulation

A water phantom with dimensions of $30 \times 30 \times 30$ cm^3 was setup in order to represent the geometry of the patient receiving external beam therapy. Ti6Al4V alloy was placed into

the water horizontally at the depth of $a = 3$ cm from surface to skip the build up region (Fig. 1). Afterwards, the water phantom was CT-scanned on GE Healthcare Optima CT520 (GE Healthcare, Waukesha, WI, USA). CT scans of the phantom were acquired sequentially using a slice thickness of 1.25 mm at a peak tube voltage of 140 kV. The experimental phantom setup and imaging procedures were also repeated for the CoCrMo alloy placed at the depth of $a = 3.5$ cm from the water surface.

2.3. Monaco TPS dose calculations

The DICOM images of the water phantom were imported into the Elekta Monaco TPS (Version 5.11.02). TPS converts the Hounsfield units on the CT images into electron density values from the CT-to-ED table for the respective tube voltage. Then the Relative Electron Density (RED) value was assigned to each voxel. To assign the mass density (ρ) to the RED the following equation was used [30].

$$\rho = (\text{RED} - 0.15)/0.85 \quad \text{RED} \geq 1. \tag{1}$$

The mass density values are converted to RED values as Monaco TPS provides accurate calculations for density values in the range up to 3 g/cm^3. As the mass density values rise above mentioned range, the accuracy of the dose accumulation decreases. Therefore, the RED value should be recalculated by using Eq. (1) [30]. The RED values for the Ti6Al4V and CoCrMo alloys used in this study were calculated as 3.92 and 7.21, respectively. Initially, the metal objects from both CT-scan data sets were contoured in Monaco TPS using known real dimensions. Then, the contours of the metal objects were contracted and expanded artificially by 2 mm, assumed to be the contouring misjudgment size, over their real dimensions in order to investigate the effect of errors in the demarcation process on the dose distribution in the ROI. Thus, each metal object was contoured in three different sizes as real, contracted, and expanded. Subsequently, recalculated RED values were assigned to the respective contours. The artifacts for real, contracted, and expanded metal implant volumes were contoured separately and the RED values were overridden as 1.0. In order to evaluate the effect of implant materials on dose distribution, the ROI was chosen as $5 \times 5 \times 5$ cm^3, located at 3 mm below the real Ti6Al4V and CoCrMo alloy volumes (Fig. 1). 6 MV photon energy beam for treatment plans were produced by the Elekta Synergy linear accelerator (Elekta, AB, Stockholm, Sweden). The field size was determined as 10×10 cm^2 at a source to surface distance (SSD) of 100 cm. For the single field 200 MU was delivered to the phantom. In Monaco TPS voxel based MC algorithm the calculation properties were set to grid size 0.12 cm and statistical uncertainty per calculation 1%.

On the other hand, to obtain the depth dose (DD) values, the same experimental setup was applied in a virtual water phantom without alloy and calculated along the central beam axis in Monaco TPS.
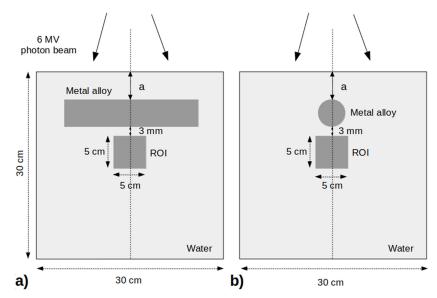
FIGURE 1. The phantom setup views of the alloys placed at a specific depth from the water surface and ROI for a) sagittal and b) coronal plane.

2.4. Ion chamber measurement

The DD values of the 6 MV photon energy of the Elekta Synergy linear accelerator were measured with a PTW 0.125 cm³ semiflex ion chamber (type 31010, PTW-Freiburg, Germany) and the field size 10×10 cm² in the water phantom.

2.5. Geant4 Monte Carlo simulation

In this study, the head model of the Elekta Synergy linear accelerator equipped with the Elekta Agility™ collimator was not simulated and the phase space data could not be obtained. At this point, the 6 MV photon energy spectrum data was taken from the study by Martins *et al*. [31] as the base. By using the reference 6 MV photon energy spectrum and the relevant source angle from the Elekta technical documents [32], the virtual water phantom ($30 \times 30 \times 30$ cm³) was irradiated with a field size of 10×10 cm² at SSD of 100 cm in Geant4. A total of 10^9 particles were simulated, G4EmStandardPhysics_option4 as a "standard" Geant4 electromagnetic physics list and 1 mm set cut parameters were used. The DD profiles were calculated from the surface of the water to 30 cm depth by using column-like scoring meshes along the central beam axis. The doses were recorded at different depths in water with 1 mm resolution. The calculated DD values were compared with the ion chamber measurement and Monaco TPS profile. Then, to be used in further simulations in this study, the energy spectrum data was modified by trial and error method to have the best match to the DD values.

The metal alloys were simulated with known composition and densities in order to evaluate the dose distributions in the ROI near Ti6Al4V and CoCrMo alloys. The alloys were individually placed in a virtual water phantom of $30 \times 30 \times 30$ cm³ at depths of 3 cm and 3.5 cm for Ti6Al4V and CoCrMo, respectively. The ROI of $5 \times 5 \times 5$ cm³ as the scorer were fixed at the position 3 mm below the real Ti6Al4V and CoCrMo alloy volumes. By using the 6 MV energy spectrum data the water phantom was simulated with similar parameters in the DD calculation in the ROI. Since the chosen ROI remained in the region where the dose profiles (inplane-crossplane) of 10×10 cm² field size were nearly flat on the plateau, only the modified spectrum verified by the DD profiles was used for all the simulations in the absent of phase space. The simulation processes were repeated individually for real, contracted and expanded configurations of the alloys.

2.6. Analysis

The different in-house programs were written (MATLAB R2020a, MathWorks®Natick Massachusetts, U.S.A.) to evaluate the spectrum and the 3D dose data on the DICOM images exported from Monaco TPS and result of the Geant4 simulations.

3. Results

By using the energy spectrum (Fig. 2), the DD values along the central axis at SSD of 100 cm with a field size of 10×10 cm² was calculated with Geant4. Then, the DD values were normalized with the maximum value of Monaco TPS. Thus, the three DD curves of Geant4, Monaco TPS and ion chamber measurement have been made suitable for comparison with each other. The 6 MV photon beam DD values for Elekta Synergy linear accelerator are fairly similar, as it is shown in Fig. 3 and the difference between them is below 1%. The detailed inset image also shows small differences between the DD values. According to the reports of the International Commission on Radiation Units and Measurements 42, the dose calculation algorithms used in TPS should aim
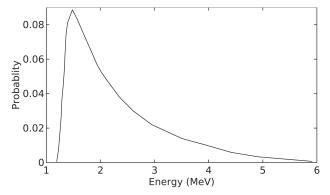
FIGURE 2. The modified 6 MV photon energy spectrum of the Elekta Synergy linear accelerator.
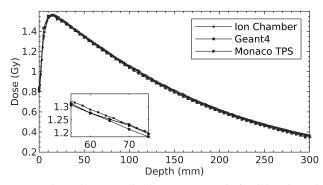

FIGURE 3. The normalized DD curves obtained by Geant4, Monaco TPS and ion chamber measurement for 6 MV photon energy. Inset: Close-up view between the depth of 55-75 mm.

at a maximum deviation of 2% from accuracy in regions with low dose changes [33].

The dose distributions along the central axis with real, contracted and expanded contouring of the alloys were evaluated in ROIs for Geant4 and Monaco TPS. As seen in Fig. 4, the local isodose values among the alloys vary up to 15%. When all the isodose graphics were considered, it was observed that each graph was symmetrical along the central beam axis. Moreover, the dose patterns for Geant4 and Monaco TPS were compatible with each other.

The dose changes with respect to depth in ROIs were evaluated for three different contours. As shown in Fig.4, the results are consistent with each other for Geant4 and Monaco TPS. The dose values are in decreasing order of contracted,

real and expanded contours. Also seen that the dose decrease is greater for CoCrMo than Ti6Al4V in all ROIs.

The dose calculations were performed in Geant4 by using the modified X-ray energy spectrum and dose values were obtained from TPS. The mean dose differences in three different size ROIs ($3 \times 3 \times 3 \, \text{cm}^3$, $4 \times 4 \times 4 \, \text{cm}^3$, $5 \times 5 \times 5 \, \text{cm}^3$) were calculated to observe the contouring effect. Table I shows the percentage mean dose differences in ROIs, depending on the different contouring sizes of Ti6Al4V and CoCrMo alloys for both Geant4 and Monaco TPS. The differences were found to be negative for real minus contracted (real - contracted) contours and positive for real minus expanded (real - expanded) contours. The greatest mean dose difference observed in $3 \times 3 \times 3 \, \text{cm}^3$. In general, the dose differences between the Geant4 and Monaco TPS calculations decrease as ROI size increases. Due to the different contouring the mean dose differences ranges from $\pm 2.4\%$ to $\pm 5.2\%$ and $\pm 3.9\%$ to $\pm 8.0\%$ for Ti6Al4V and CoCrMo alloys, respectively.

4. Discussion

The DD values obtained from Geant4 simulation were well-matched to ion chamber measurements and Monaco TPS calculations. However, despite using the estimated energy spectrum, a certain dose difference occurred between Geant4 and Monaco TPS in all contouring configurations. This is similar to the results of the study in which the dose discrepancies of up to 9.5% were attained in the shadow of inhomogeneity [34]. In addition, it has been shown in previous studies that the differences between measurements at a certain depth and TPS algorithms cause dose uncertainties of $5 - 23\%$ [1, 14, 24–28]. However, a better match between measurements and simulations with full linear accelerator head simulation could be achieved if all the details were available. While the main method is still the full modeling of the linear accelerator head, using a modified energy spectrum for MC simulations where geometric details, verified phase space and energy spectrum were not available offers an alternative [31].

The dose distributions in contouring of alloys in different sizes were analyzed with the isodose and the DD graphs in the ROIs. While the isodose values of Geant4 and Monaco TPS created by the beams passing through the edges of the

TABLE I. The percentage mean dose differences due to contour sizes (± 2 mm).

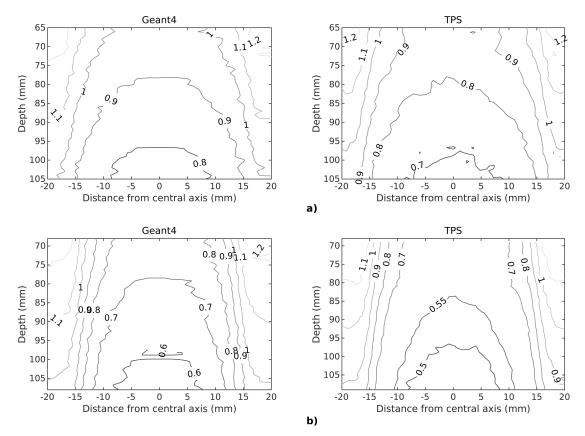| ROI size $\left(\text{cm}^3\right)$	Ti6Al4V alloy				CoCrMo alloy			
	Mean dose differences %				Mean dose differences %			
	Real-Contracted		Real-Expanded		Real-Contracted		Real-Expanded	
	Geant4	TPS	Geant4	TPS	Geant4	TPS	Geant4	TPS
$3 \times 3 \times 3$	−3.1	−5.2	3.4	5.0	−6.5	−8.0	6.1	7.1
$4 \times 4 \times 4$	−2.8	−4.4	2.8	4.4	−4.8	−6.1	5.0	5.7
$5 \times 5 \times 5$	−2.4	−3.4	2.4	3.8	−3.9	−5.1	4.0	4.5

FIGURE 4. The isodose graphics of a) Ti6Al4V b) CoCrMo alloys shown here only contoured to their real dimensions along the central beam axis.
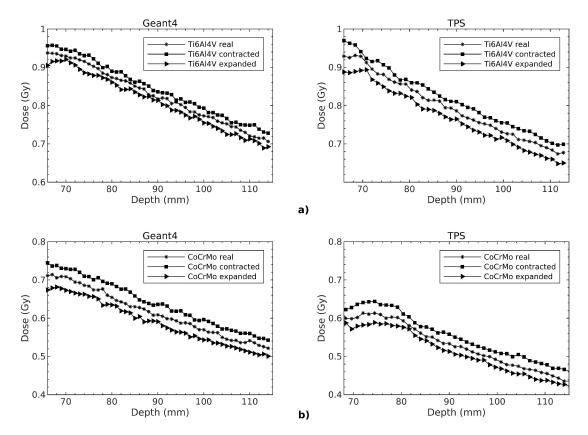

FIGURE 5. The DD curves in ROIs near metal alloys contoured as real, contracted, and expanded.

irradiated metal alloys are in good agreement, the certain differences have been found in the regions under the shadow of the metal alloys. Because, distortion occurs in the absorbed dose distribution due to the attenuation of the beam and the interactions at the tissue-metal interface when the incident photon passes through the metallic implant [1]. This effect decreases when the metal alloys are contoured as contracted and increases as expanded. Compton scattering is the dominant type of interaction that occurs between MeV photons and high-density heterogeneities. Independent of effective atomic number (Z_{eff}), the number of these interactions increases with electron density [35]. Therefore, the entrance dose of ROI which depend on the density of the alloy was higher for Ti6Al4V alloy compared to CoCrMo alloy for both Geant4 and Monaco TPS.

The percentage mean dose differences in Table I show that the CoCrMo alloy absorbed more energy and created more heterogeneous dose distribution in the closer region due to the higher bulk and electron density [36]. Hence, the percentage mean dose differences of CoCrMo were greater than of Ti6Al4V among all contours. To avoid the edge effect of the beam, small volume ROIs such as $3 \times 3 \times 3$ cm^3, $4 \times 4 \times 4$ cm^3, $5 \times 5 \times 5$ cm^3 were chosen and placed at a certain distance from the alloys along the central beam axis. The percentage mean dose differences calculated in $3 \times 3 \times 3$ cm^3 ROIs were the highest in all contouring configurations. Since the ROIs were closer to metal alloys, the scattering contribution from them is higher to the dose. Accordingly, the dose differences between Geant4 simulation and Monaco TPS calculations decreased as the ROI volume increased and as the metal alloys moved away. In the experimental study of Byrnes *et al.*, the percentage of mean dose differences between the TPS calculations and measured in the small field size in the dose shadow of blocks with a total metal thickness of 3 cm were evaluated. The dose differences calculated by exact contouring increased as the density of the material increased. Thus, the results are compatible without exact delineation of implants [14].

As a result, the limitations in determining the contours of metal alloys that cause artifacts in CT images led to errors in dose calculations. This study shows that ± 2 mm error in determining the boundaries of metal alloys caused up to $\pm 8\%$ differences in the dose calculations in a close region, depending on the density of the material consisting of uniform cylindrical geometry. If the existing material does not have a uniform geometry, the borders will be contoured as contracted in some cases and expanded in some other. In this case, the dose calculation error would be higher in a region close to the alloy.

5. Conclusion

The dose distortions in radiotherapy due to artifacts caused by high atomic number materials have been calculated with TPS and compared with MC simulations to evaluate these dose changes in a detailed and reliable way. It has been found that the mistakes made in contouring high density materials cause significant dose differences. Even these errors of a few millimeters in contouring can lead to increased doses of organs at risk in the treatment region or lower doses in the target volume. This will become increasingly important, especially in situations where the overlap between target volume and metal implants is large. Thus, it can have a significant negative impact on patient outcomes. This study emphasized the importance of the effect of implant composition and contouring size on dose distributions in a region close to the material. Thus, it will eliminate one aspect of the uncertainty in the planning process. Therefore, materials with high atomic numbers in the patient's CT images should be contoured very carefully and their mass density values should be assigned to TPS [11]. In further studies, it is desired to evaluate the dose differences in non-uniform geometries in regions close to high density materials.

1. C. Reft *et al.*, *Dosimetric considerations for patients with HIP prostheses undergoing pelvic irradiation, Report of the AAPM Radiation Therapy Committee Task Group 63*, Med. Phys. **30** (2003) 1162, https://doi.org/10.1118/1.1565113.

2. G.X. Ding, C.W. Yu, *A study on beams passing through hip prosthesis for pelvic radiation treatment*, Int. J. Radiat. Oncol. Biol. Phys. **51** (2001) 1167, https://doi.org/10.1016/s0360-3016(01)02592-5.

3. M.B. Hazuka, G.S. Ibbott, J.J. Kinzie, *Hip prostheses during pelvic irradiation: Effects and corrections*, Int. J. Radiat. Oncol. Biol. Phys. **14** (1988) 1311, https://doi.org/10.1016/0360-3016(88)90412-9.

4. P.J. Biggs, M.D. Russell, *Effect of a femoral head prosthesis on megavoltage beam radiotherapy*, Int. J. Radiat. Oncol. Biol. Phys. **14** (1988) 581, https://doi.org/10.1016/0360-3016(88)90279-9.

5. S.E. Schild, J.S. Robinow, H.E. Casale, L.P. Bellefontaine, S.J. Buskirk, *Radiotherapy treatment planning for prostate cancer in patients with prosthetic hips*, Med. Dosim. **17** (1992) 83, https://doi.org/10.1016/0958-3947(92)90018-b.

6. R. Alecu, M. Alecu, T. Loomis, T. Ochran, T. He, *Traditional and MLC based dose compensator design for pa-

tients with hip prostheses undergoing pelvic radiation therapy, Med. Dosim. **24** (1999) 33, https://doi.org/10.1016/s0958-3947(98)00044-2.

7. M. Carolan, P. Dao, C. Fox, P. Metcalfe, *Effect of hip prostheses on radiotherapy dose*, Australas. Radiol. **44** (2000) 290, https://doi.org/10.1046/j.1440-1673.2000.00816.x.

8. K-P. Chang, W-T. Lin, A-C. Shiau, Y-H. Chie, *Dosimetric distribution of the surroundings of different dental crowns and implants during LINAC photon irradiation*, Radiat. Phys. Chem. **104** (2014) 339, https://doi.org/10.1016/j.radphyschem.2013.11.026.

9. S. Spirydovich, L. Papiez, M. Langer, G. Sandison, V. Thai, *High density dental materials and radiotherapy planning: Comparison of the dose predictions using superposition algorithm and fluence map Monte Carlo method with radiochromic film measurements*, Radiother. Oncol. **81** (2006) 309, https://doi.org/10.1016/j.radonc.2006.10.010.

10. S.A.M. Lloyd, W. Ansbacher, *Evaluation of an analytic linear Boltzmann transport equation solver for high-density inhomogeneities*, Med. Phys. **40** (2013) 011707, https://doi.org/10.1118/1.4769419.

11. E. Buffard, R. Gschwind, L. Makovicka, C. David, *Monte Carlo calculations of the impact of a hip prosthesis on the dose distribution*, Nucl. Instruments Methods Phys. Res. Sect. B Beam Interact. with Mater. Atoms **251** (2006) 9, https://doi.org/10.1016/j.nimb.2006.05.031.

12. N. Ade, F.C.P. du Plessis, *Monaco and film dosimetry of 3D CRT, IMRT and VMAT cases in a realistic pelvic prosthetic phantom*, Radiat. Phys. Chem. **145** (2018) 50, https://doi.org/10.1016/j.radphyschem.2017.11.013

13. D.G. Kovacs *et al.*, *Metal artefact reduction for accurate tumour delineation in radiotherapy*, Radiother. Oncol. **126** (2018) 479, https://doi.org/10.1016/j.radonc.2017.09.029.

14. K. Byrnes, A. Ford, N. Bennie, *Verification of the Elekta Monaco TPS Monte Carlo in modelling radiation transmission through metals in a water equivalent phantom*, Australas. Phys. Eng. Sci. Med. **42** (2019) 639, https://doi.org/10.1007/s13246-019-00749-2.

15. T. Krieger, O.A. Sauer, *Monte Carlo-versus pencil-beam-/collapsed-cone-dose calculation in a heterogeneous multilayer phantom*, Phys. Med. Biol. **50** (2005) 859, https://doi.org/10.1088/0031-9155/50/5/010.

16. B.J. Mijnheer, *The clinical basis for dosimetric accuracy in radiotherapy, In Radiation incidents: Uncertainties, errors and accidents in radiotherapy*, British Institute of Radiology, (London, 1996) pp16.

17. G.H. Fletcher, Textbook of Radiotherapy, 3rd ed. (Lea and Febiger, Philadelphia, 1980).

18. A. Bujold, T. Craig, D. Jaffray, L.A. Dawson, *Image-Guided Radiotherapy: Has It Influenced Patient Outcomes?*, Semin. Radiat. Oncol. **22** (2012) 50, https://doi.org/10.1016/j.semradonc.2011.09.001.

19. N. Papanikolaou, J.J. Battista, A.L. Boyer, C. Kappas, E. Klein, T.R. Mackie, *AAPM report 85: Tissue Inhomogeneity Corrections for Megavoltage Photon Beams, Report of the AAPM radiation therapy committee task group 65*, (2004).

20. A. Bielajew, Monte Carlo Techniques in Radiation Therapy, (In: J. Seco, F. Verhaegen, editors, Boca Raton: CRC Press, 2013), pp. 3-16.

21. T. Han, J.K. Mikell, M. Salehpour, F. Mourtada, *Dosimetric comparison of Acuros XB deterministic radiation transport method with Monte Carlo and model-based convolution methods in heterogeneous media*, Med. Phys. **38** (2011) 2651, https://doi.org/10.1118/1.3582690.

22. A. Fogliata *et al.*, *On the dosimetric behaviour of photon dose calculation algorithms in the presence of simple geometric heterogeneities: Comparison with Monte Carlo calculations*, Phys. Med. Biol. **52** (2007) 1363, https://doi.org/10.1088/0031-9155/52/5/011.

23. E. Sterpin, M. Tomsej, B. De Smedt, N. Reynaert, S. Vynckier, *Monte Carlo evaluation of the AAA treatment planning algorithm in a heterogeneous multilayer phantom and IMRT clinical treatments for an Elekta SL25 linear accelerator*, Med. Phys. **34** (2007) 1665, https://doi.org/10.1118/1.2727314.

24. N. Ade, F.C.P. du Plessis, *Dose comparison between Gafchromic film, XiO, and Monaco treatment planning systems in a novel pelvic phantom that contains a titanium hip prosthesis*, J. Appl. Clin. Med. Phys. **18** (2017) 162, https://doi.org/10.1002/acm2.12141.

25. R. Prabhakar, M. Kumar, S. Cheruliyil, S. Jayakumar, S. Balasubramanian, J. Cramb, *Volumetric modulated arc therapy for prostate cancer patients with hip prosthesis*, Reports Pract. Oncol. Radiother. **18** (2013) 209, https://doi.org/10.1016/j.rpor.2013.03.006.

26. W.L. Ng *et al.*, *Volumetric modulated arc therapy in prostate cancer patients with metallic hip prostheses in a UK centre*, Reports Pract. Oncol. Radiother. **20** (2015) 273, https://doi.org/10.1016/j.rpor.2015.03.006.

27. J.D. Rijken, C.J. Colyer, *Dose uncertainties associated with a set density override of unknown hip prosthetic composition*, J. Appl. Clin. Med. Phys. **18** (2017) 301, https://doi.org/10.1002/acm2.12167.

28. M. Sasaki *et al.*, *Dosimetric Verification around High-density Materials for External Beam Radiotherapy*, Nihon Hoshasen Gijutsu Gakkai Zasshi **72** (2016) 735, https://doi.org/10.6009/jjrt.2016_jsrt_72.9.735.

29. S. Agostinelli *et al.*, *GEANT4 - A simulation toolkit*, Nucl. Instruments Methods Phys. Res. Sect. A Accel. Spectrometers, Detect. Assoc. Equip. **506** (2003) 250, https://doi.org/10.1016/s0168-9002(03)01368-8.

30. IMPAC Medical System Inc, Monaco dose calculation technical reference, Sunnydale, 2013.

31. J.C. Martins *et al.*, *Optimization of Phase Space files from clinical linear accelerators*, Phys. Medica **64** (2019) 54, https://doi.org/10.1016/j.ejmp.2019.06.007.

32. Elekta Agility™ and Integrity™ R3.1., Instructions for Use-Clinical Mode, 2013, pp. 203–5.

33. J. Van Dyk, R.B. Barnett, J.E. Cygler, P.C. Shragge, *Commissioning and quality assurance of treatment planning computers*, Int. J. Radiat. Oncol. Biol. Phys. **26** (1993) 261, https://doi.org/10.1016/0360-3016(93)90206-b

34. T. Kairn *et al.*, *Dosimetric effects of a high-density spinal implant*, Journal of Physics: Conference Series **444** (2013) 012108, `https://doi.org/doi:10.1088/1742-6596/444/1/012108`.

35. F.M. Khan, The Physics of Radiation Theraphy, 5th ed. (Lippincott Williams and Wilkins, Philadelphia, 2014)

36. D. Akçay, *The effect of prosthesis implant materials on doses in external beam treatment comparison with different dose calculation algorithms and dosimetry in phantom model*, Master's Theses, Dokuz Eylul University, 2013.